Clinical Radiology 74 (2019) 933–943

Contents lists available at ScienceDirect

Clinical Radiology

journal homepage: www.clinicalradiologyonline.net

A radiomics model for determining the invasiveness of solitary pulmonary nodules that manifest as part-solid nodules

Q. Weng [a,1], L. Zhou [b,1], H. Wang [a], J. Hui [a], M. Chen [a], P. Pang [c], L. Zheng [a], M. Xu [a], Z. Wang [a], J. Ji [a,*]

[a] *Key Laboratory of Imaging Diagnosis and Minimally Invasive Intervention Research, Lishui Hospital of Zhejiang University, Lishui, 323000, China*
[b] *Department of Radiology, Lishui People's Hospital, Lishui, 323000, China*
[c] *GE Healthcare, Hangzhou 310000, China*

ARTICLE INFORMATION

Article history:
Received 18 April 2019
Accepted 31 July 2019

AIM: A nomogram model was developed to predict the histological subtypes of lung invasive adenocarcinomas (IAs) and minimally invasive adenocarcinomas (MIAs) that manifest as part-solid ground-glass nodules (GGNs).

MATERIALS AND METHODS: This retrospective study enrolled 119 patients with histopathologically confirmed part-solid GGNs assigned to the training (n=83) or testing cohorts (n=36). Radiomic features were extracted based on the unenhanced computed tomography (CT) images. R software was applied to process the qualitative and quantitative data. The CT features model, radiomic signature model, and combined prediction model were constructed and compared.

RESULTS: A total of 396 radiomic features were extracted from the preoperative CT images, four features including MaxIntensity, RMS, ZonePercentage, and LongRunEmphasis_angle0_offset7 were indicated to be the best discriminators to establish the radiomic signature model. The performance of the model was satisfactory in both the training and testing set with areas under the curve (AUCs) of 0.854 (95% confidence interval [CI]: 0.774 to 0.934) and 0.813 (95% CI: 0.670 to 0.955), respectively. The CT morphology of the lesion shape and diameter of the solid component were confirmed to be a significant feature for building the CT features model, which had an AUC of 0.755 (95% CI: 0.648 to 0.843). A nomogram that integrated lesion shape and radiomic signature was constructed, which contributed an AUC of 0.888 (95% CI: 0.82 to 0.955).

CONCLUSIONS: The radiomic signature could provide an important reference for differentiating IAs from MIAs, and could be significantly enhanced by the addition of CT morphology. The nomogram may be highly informative for making clinical decisions.

* Guarantor and correspondent: J. Ji, Key Laboratory of Imaging Diagnosis and Minimally Invasive Intervention Research, Lishui Hospital of Zhejiang University, School of Medicine, Lishui, Zhejiang, 323000, China. Tel./fax: +86 0578 2285011.
E-mail address: lschrjjs@163.com (J. Ji).
[1] These authors contributed equally to this work.

https://doi.org/10.1016/j.crad.2019.07.026

Introduction

Lung cancer remains the leading cause of cancer-related death globally,[1] and adenocarcinoma is the most common histological type of lung cancer and frequently presents as ground-glass nodules (GGNs) on computed tomography (CT).[2] The evaluation of GGNs has become an important topic due to the high malignancy rate of persistent GGNs. In clinical practice, GGNs are detected in 0.2%–0.5% of the scanned population,[3] and this prevalence continues to escalate as the use of CT becomes widespread. Based on the fact that the long-term course of pure GGNs (pGGNs) seems to be relatively indolent,[4] the Fleischner Society guidelines recommended follow-up scans at 6–12 months after diagnosis and then every 2 years thereafter until 5 years after diagnosis for pGGNs 6 mm or larger.[5] Part-solid nodules have been considered to have a higher likelihood of malignancy than pGGNs or solid nodules,[6] with a malignancy rate as high as 63%.[7] If a malignancy is suspected, additional therapies are recommended in a multidisciplinary approach. The management of part-solid nodules, however, varies greatly based on the invasiveness of the nodule.[8]

According to the pathological classification by the World Health Organization (WHO), lung adenocarcinoma and its precursor lesions are classified into the following: atypical adenomatous hyperplasia (AAH), adenocarcinoma in situ (AIS), minimally invasive adenocarcinomas (MIA), and invasive adenocarcinomas (IAs).[9] When GGNs represent AAH or AIS, tumours grow along the alveolar walls only to appear as homogeneous GGNs at CT, both of which provide the most favourable prognoses.[10] Sublobar resection, such as segmentectomy and wedge resection, is applicable for MIAs, with approximately 100% 5-year disease-free survival after complete resection.[11] Standard lobectomy and extensive lymph node dissection are recommended for patients who present with IAs.[12] The 5-year disease-free survival of IAs is 74.6%,[13] which is considered to be intermediate or high-grade clinical behaviour[14]; however, part-solid nodules remain a diagnostic challenge. It is clinically important to differentiate MIAs from IAs prior to surgery as the distinction could favourably affect clinical decision-making.

The definitive diagnosis of a lesion requires in-depth histological evaluation of the entire tumour specimen, and it is challenging to diagnose lesions with certain histopathological subtypes.[15] Medical imaging is in routine use in oncology for detecting tumours, defining tumour locations, the extent of disease, treatment planning, and longitudinal response monitoring.[16] CT images display strong feature differences between lesion subtypes that can be used to differentiate between GGNs.[17] Imaging studies can provide additional information that biopsies fail to deliver, such as radiographic intratumour heterogeneity, as well as monitor patient response during treatment. Hence, if MIAs and IAs can be diagnosed correctly using radiological images in advance, patients would be better managed using precise treatment strategies.

Radiomics is a process designed to extract innumerable high-dimensional mineable data from radiological images using automated data characterisation algorithms.[18] Radiomics makes if possible to provide personalised and precision medicine non-invasively and cost-effectively.[19–21] Increasing numbers of pattern recognition tools and dataset sizes have facilitated the development of processes for radiomics.[22] Philipp *et al.* proved that an 11-feature radiomic signature allows for the prediction of survival and stratification of patients with newly diagnosed glioblastomas and outperforms established clinical and radiological risk models.[23] Radiomics has been applied to decode tumour phenotypes, histological subtypes of lung adenocarcinoma, and even the pathological response of non-small cell lung cancer.[24]

The present study established an integrated signatures model that combines CT features with radiomics signatures, which can be used to differentiate IAs from MIAs that present as part-solid nodules based on unenhanced CT.

Materials and methods

Patient cohort

The Institutional Review Board of two institutions approved the study and waived the requirement for informed consent. Data were included from 119 solitary part-solid nodules that were histopathologically confirmed before treatment from February 2014 to December 2016. The inclusion criteria were as follows: (a) patients >18 years old; (b) patients with nodules that were between 5–30 mm in diameter. According to the IASLC/ATS/ERS classification, an MIA is described as a nodule <30 mm in diameter with a predominant lepidic pattern that harbours an invasive area measuring <5 mm composed of any subtype of IA. An IA is defined by the presence of an invasive component >5 mm[25]; (c) patients with solitary part-solid nodules; (d) patients who did not undergo preoperative treatment; and (e) patients who underwent surgical resection within 1 month of CT.

CT examination and imaging analysis

All preoperative unenhanced CT examinations were performed on 64-channel Philips Brilliance CT system (Philips Medical Systems, Eindhoven, The Netherlands). The imaging acquisition parameters were as follows: 120 kV tube voltage; 200 mA tube current; 40 mm (64×0.625 mm) collimation width; 0.9 mm section thickness; 0.45 mm reconstruction interval with iDose3 hybrid iterative reconstruction algorithm; 15–20 cm SFOV; 1.2 pitch; 350 ms rotation time; and 1024×1024 pixels matrix size. The images were processed in an Extended Brilliance Workspace (EBW, Philips). Multiplanar reconstruction was used for image reconstruction with a thickness of 5 mm. Both lung window (width, 1,500 HU; level, −650 HU) and mediastinal window (width, 400 HU; level, 40 HU) imaging were obtained.

The CT images were reviewed independently by two thoracic radiologists with 8 and 12 years of experience. Any

disagreement was settled by the third radiologist who had 15 years of experience. The image features included the following: (a) lesion diameter: for part-solid nodules, the CT sections chosen for measurements were those that displayed the largest portion of the overall nodule and the solid component; (b) lesion area; (c) diameter of the solid component; (d) area of the solid component[26]; (e) shape: regular (round or oval) or irregular[27]; (f) attenuation value; (g) presence of vacuoles (single or multiple cystic cavity with diameters <5 mm)[28]; (h) presence of an air bronchogram; (i) lesion margin: smooth, lobulate, or spiculate; (j) lesion border; and (k) lesion location were interpreted. Clinical data of the enrolled patients were collected from the electronic data system.

Tumour segmentation

The CT images were retrieved from the picture archiving and communication system (PACS) using the keyword "GGN". The ITK-SNAP software (www.itk-snap.org) was used for semi-automatic segmentation. All regions of interest (ROIs) were manually drawn on the CT images on each section as an area that was as large as possible from all sections to cover the target nodule. The reproducibility of the intra-observer and interobserver segmentation was confirmed by two experienced thoracic radiologists with 10 years and 13 years of experience, respectively.

Texture feature extraction

Artificial Intelligence Kit software (A.K. software; GE Healthcare, China) was employed to extract the CT image features. A total of 396 radiomic features from each patient were generated based on the following four categories: Histogram, Formfactor, Grey-level size zone matrix (GLSZM), and Run-length matrix (RLM). Forty-five histogram-based features reflected the intensity information of a given ROI.[29] Nine form factor-based parameters described the three-dimensional size and shape of the tumour region. One hundred and sixty-two GLSZM-based features represented the joint probability of certain sets of pixels having certain grey-level values, and the co-occurring pairs of pixels could be spatially related in various orientations relative to distance (1,4,7 displacement) and angular (0°,45°, 90°, 135°) spatial relationships to represent the intensity value of a neighbourhood.[30] One hundred and eighty RLM-based features were defined as the number of runs with pixels of different grey levels and run lengths for a given direction such as those defined by GLCM.[31] The extracted texture features were standardised by Z-score ($z = \frac{x-\mu}{\sigma}$, where μ was the mean value of the images, and σ was the standard deviation), which could remove the unit limits on the data of each feature. Then, the outliers, "nan", were replaced with the median of the parameter.

Feature selection and radiomics signature construction

The patients were divided into the training cohort (n=83) and the validation cohort (n=36) with a ratio of 7:3.[32] The training data were used to build the radiomics model. To reduce overfitting or selection bias in the radiomics model, the dimension reduction was achieved in three steps. First, analysis of variance (ANOVA; for normally distributed features) and Mann–Whitney *U*-tests (for abnormally distributed features) were used to select the significant features (144 features). Second, an inter-feature coefficient was calculated to identify the highest correlated features to the principal features that described at least 90% of the variance in the radiomics data to reduce data redundancy. This resulted in a selection of 31 variance-retaining features. Third, the least absolute shrinkage and selection operator (LASSO) was used to further select features by penalty parameter tuning and 10-fold cross-validation based on the minimum criteria, and the final four features were selected. A linear regression of the selected features was used to build the radiomics signature and calculate the radiomics score (Rad-score) for each patient. The non-zero coefficient of the selected feature is defined as the Rad-score. The Rad-score was calculated for each patient as a linear combination of the selected features weighted by their respective coefficients based on the following formula:

$$\text{Rad-score} = -0.731 \times \text{MaxIntensity} + 0.454 \times \text{RMS} - 3.389 \times \text{Zone Percentage} + 0.76 \times \text{LongRunEmphasis\_angle0\_offset7} - 1.32.$$

The predictive accuracy of the radiomics signature was quantified by the area under the receiver operator characteristic (ROC) curve (AUC) in both the training and testing sets.

Construction and assessment of the radiomics nomogram

In the training data, univariate logistic regression analyses were performed for each potential predictive variable, such as lesion diameter, lesion area, diameter of the solid component, area of the solid component, lesion shape, patient sex, patient age, primary tumour site, CT value, presence of vacuoles, presence of an air-bronchogram, lesion margin, and lesion border to select the independent clinical predictors. A multivariable logistic regression analysis combining the independent clinical risk factors and radiomic signatures was applied to develop a diagnostic model. A radiomics nomogram was then constructed based on the multivariate logistic regression model. The calibration of the nomogram was assessed with a calibration curve. Furthermore, to evaluate the discriminatory ability of the nomogram, ROC curves were developed. A radiomics score was calculated for each patient in the testing set using the formula constructed in the training set. The calibration curve was generated and the AUC was calculated.

The intra-observer and interobserver agreement

The intra-observer and interobserver agreements of feature extraction and CT feature characterisation were evaluated by intraclass correlation coefficients (ICCs). Initially 30 random CT images were chosen for ROI segmentation, feature extraction, and CT feature characterisation. ROI segmentation and CT feature characterisation were

performed by two experienced radiologists independently. The intra-observer ICC was computed by comparing two extractions of reader A separated by a 1-month interval. The interobserver ICC was computed by comparing the extractions of reader B with 15 years of experience and the first extraction of reader A within 2 weeks. When the ICC was greater than 0.75, it was considered good agreement, and the remaining image segmentation was performed by reader A.

Statistical analysis

All quantitative features were performed with R software (version 3.3). The variable distribution was examined by the Kolmogorov–Smirnov test, and Student's *t*-test was used to determine whether the characteristic features were significantly different between the MIA and IA groups for normally distributed features; otherwise, the Mann–Whitney *U*-test was used. The statistically significant clinical/morphological characteristics and the radiomic signatures were used as the input variables for multivariable logistic regression analysis to identify independent predictors. A significance threshold of $p<0.05$ was set. All the variables that showed statistical significance in the univariate analysis were used in multivariate analysis to look for predictors of efficacy. A nomogram was established by incorporating all significant predictors. ROC curves were plotted to evaluate the diagnostic efficiency of the model. The AUC was calculated.

The multivariate binary logistic regression was performed with the "rms" package. The nomogram construction and calibration plots were performed using the "rms" package.

Results

Demographic and clinical findings

The part-solid nodules were reviewed in the picture archiving and communication system (PACS) and histopathologically confirmed in 672 patients. A total of 119 patients with solitary part-solid nodules (≤3 cm) were enrolled in this retrospective study according to the inclusion and exclusion criteria. Of the 119 nodules, 70 were IAs, and 49 were MIAs. Patients were randomly assigned to the training cohort (49 IAs and 34 MIAs) or the testing cohort (21 IAs and 15 MIAs), as shown in Fig 1.

The demographic and clinical characteristics of the final study population are summarised in Table 1. The median age of the population in the training cohort was 58.50 (52.75, 68.50) years for patients with MIAs and 64.0 (51.0, 70.50) years for patients with IAs, while in the testing cohort, the mean age was 59.13±8.63 years for patients with MIA and 63.76±10.51 for patients with IA. Significant differences were found in lesion diameter ($p=0.001$), lesion area ($p=0.001$), diameter of the solid component ($p=0.001$), area of the solid component ($p<0.01$), lesion shape ($p<0.001$), CT value ($p<0.001$), presence of vacuoles ($p=0.025$), presence of an air-bronchogram ($p=0.002$), lesion margin ($p<0.001$), and lesion border ($p<0.001$) in the training sets. In multivariate analysis, diameter of the solid component ($p=0.022$) and lesion shape ($p=0.003$) were found to be significant in differentiating MIAs and IAs (data not shown), meaning that the part-solid nodules with longer diameters and irregular shapes are more likely to be IAs. The input selection was used to build the CT features model and showed that lesion shape was the most useful indicator for differentiating between MIAs and IAs ($p=0.004$).

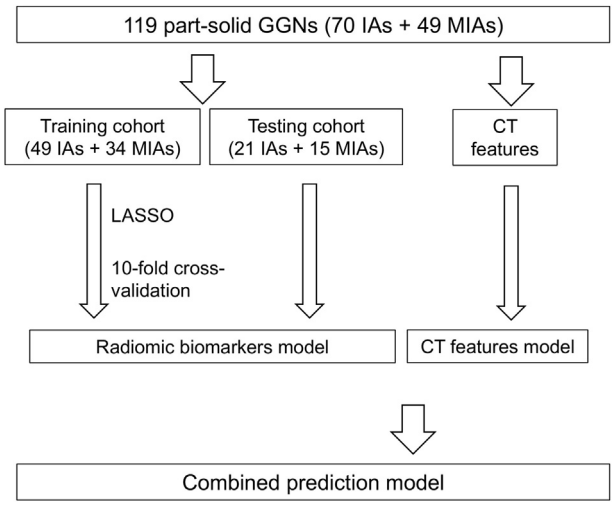

Figure 1 Flow chart for building the prediction model.

Interobserver and intra-observer reproducibility

There were no statistically significant differences between the measurements of the two readers for each selected feature, with *p*-values ranging from 0.712 to 0.861 for radiomic feature extraction and 0.781 to 0.873 for CT feature characterisation. The intra-observer ICCs calculated based on two measurements were good, ranging from 0.81 to 0.96 for radiomic feature extraction and 0.79 to 0.88 for CT feature characterisation. The interobserver agreement between two readers ranged from 0.78 to 0.92 for radiomic feature extraction and 0.83 to 0.94 for CT feature characterisation. The results indicated favourable intra- and interobserver reproducibility of feature extraction and CT feature characterisation. Therefore, all outcomes were based on the measurement of the first reader (reader A).

Radiomic score and radiomic model construction

A total of 396 radiomic features were extracted by A.K. software. Student's *t*-test was used when the data satisfied a normal distribution; otherwise, the Mann–Whitney *U*-test was used, and 144 radiomic features were retained. After Spearman analysis using $|r|=0.9$, only 31 radiomic features were retained (Fig 2). The most valuable four radiomic features (Fig 3a and b) were selected by 10-fold cross-validation with LASSO, which can be applied for biomarker selection in high-dimensional data. The

Table 1
Characteristics of the patients in the training and testing sets.

Variables	Training cohort			Testing cohort		
	MIAs (n=34)	IAs (n=49)	p-Value	MIAs (n=15)	IAs (n=21)	p-Value
Patient age	58.50 (52.75,68.50)	64.0 (51.0,70.5)	0.219	59.13±8.63	63.76±10.51	0.171
Patient sex			0.128			0.265
Male	6	16		7	6	
Female	28	33		8	15	
Lesion diameter	1.30 (1.00,1.68)	1.80 (1.40,2.35)	0.001	1.59±0.63	1.96±0.62	0.085
Lesion area	1.05 (0.62,2.02)	2.07 (1.22,4.07)	0.001	1.62 (0.72,2.24)	2.07 (1.49,4.42)	0.030
Diameter of the solid component	0.85 (0.45,1.23)	1.4 (0.9,2.1)	0.001	1.03±0.68	1.75±0.72	0.005
Area of the solid component	0.32 (0.08,0.84)	1.18 (0.54,2.74)	<0.001	0.40 (0.15,1.26)	1.78 (0.92,3.80)	0.001
Lesion shape			<0.001			0.078
Regular	20	3		6	2	
Irregular	14	46		9	19	
Attenuation	−133.50 (−293.50, −35.75)	−12.0 (−70.5,40.5)	<0.001	−288 (−354,13)	19.0 (−41.5,57.5)	0.007
Vacuole			0.025			0.028
Present	6	20		9	5	
Absent	28	29		6	16	
Air-bronchogram			0.002			0.091
Present	12	34		5	13	
Absent	22	15		10	8	
Lesion margin						
Smooth	19	9	<0.001	8	3	0.032
Lobulate	22	47	<0.001	12	21	0.126
Spiculate	12	35	0.001	6	14	0.112
Lesion border			<0.001			0.032
Clear	20	9		8	3	
Unclear	14	40		7	18	
Lesion location			0.591			0.527
Left upper lobe	5	10		2	7	
Left middle lobe	0	0		0	0	
Left lower lobe	4	6		1	3	
Right upper lobe	16	17		8	8	
Right middle lobe	5	5		1	1	
Right lower lobe	4	11		3	2	

Data are expressed as the median (quartile) or mean ± standard deviation.
A statistically significant difference is indicated by a p-value <0.05.
MIA, minimally invasive adenocarcinoma; IA, Invasive adenocarcinoma.

importance of the four features is shown in Fig 3c with their exact coefficient values shown in Table 2.

The Rad-score and calibration plot for each patient in the training and testing cohorts indicated significant differences between the IAs and MIAs (Fig 4). The radiomic features showed excellent predictive performance for discriminating IAs from MIAs in the training set and testing set (Fig 5). In the training cohort, the radiomic signature yielded an AUC of 0.854 (95% CI: 0.774 to 0.934) with 94.1% specificity. In the testing cohort, the radiomic signature yielded an AUC of 0.813 (95% CI: 0.670 to 0.955) with 100% specificity.

Comparison of the performance of the radiomic model and CT features model

Logistic regression analyses were used, only the shape and diameter of the solid component were retained as a significant CT feature. Then, the CT feature model was built with the lesion shape and diameter of the solid component (Fig 6a) and yielded an AUC of 0.755 (95% CI: 0.648 to 0.843) with 95.90% specificity and 52.90% sensitivity. The radiomic signatures model outperformed the CT feature model with a greater AUC of 0.854 (95% CI: 0.775 to 0.934). For

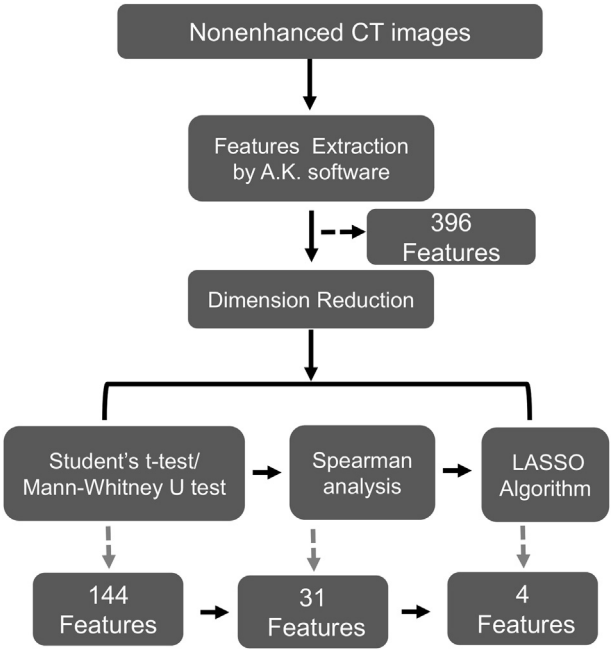

Figure 2 Feature selection process.

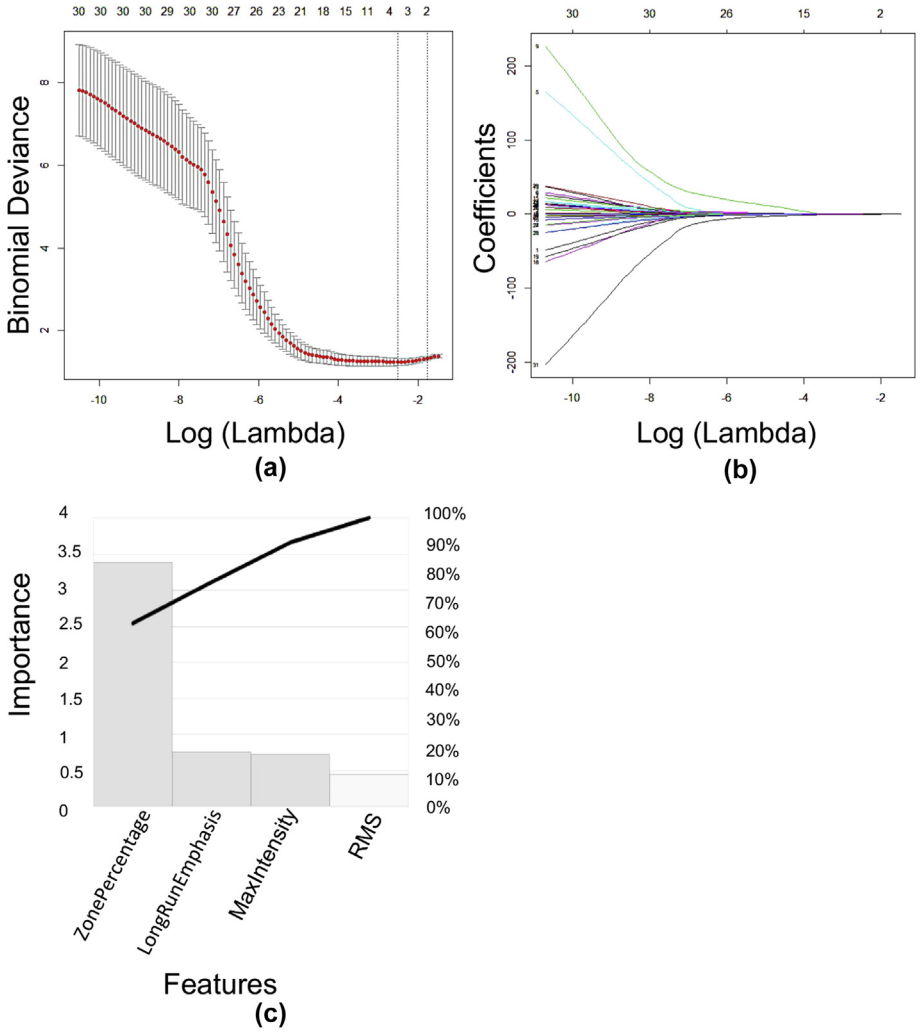

Figure 3 Feature selection and dimension reduction. (a) The 10-fold cross-validation of the LASSO analysis was applied to acquire the most valuable features when the minimum Lambda was 0.0809. (b) The regression coefficients of LASSO. (c) The importance of the four features.

construction of combined model, multivariable logistic regression analysis was employed for Rad-score and CT features (shape and diameter of the solid component). The diameter of the solid component was eliminated with *p*-value of 0.323. The performance in the combined prediction model, which incorporated the CT feature (shape) and radiomics signatures, significantly surpassed the performance of radiomics model or CT features model alone and yielded an AUC of 0.888 (95% CI: 0.820 to 0.955) with 94.1% specificity and 73.50% sensitivity (Table 3).

Table 2
The coefficients of the four selected features.

Category	Feature selected	Coefficient
Histogram	Maximum Intensity	−0.731
	RMS	0.454
GLSZM	ZonePercentage	−3.389
RLM	LongRunEmphasis_angle0_offset7	0.76
	Constant	−1.32

Construction of the predictive nomogram

A nomogram was constructed based on the results of the multivariate analysis and by the regression modelling strategies package in the R software. The radiomic score and lesion shape were integrated into the nomogram (Fig 6b). The following is an example scenario to calculate the total points and predict the possibility of a lesion being an IA: a patient with one part-solid nodule in the lung that exhibited an irregular shape (irregular: 1, means neither oval nor round) scored 7.5 points. The unenhanced CT images were imported into the A.K. software, and the Rad-score was calculated to be 2, which indicated a score of 92.5. In total, this patient had approximately 100 points on the nomogram. Theoretically, the possibility of this part-solid nodule being an IA is over 95%.

Discussion

In the present study, a diagnostic, radiomics signature-based nomogram was developed and validated for

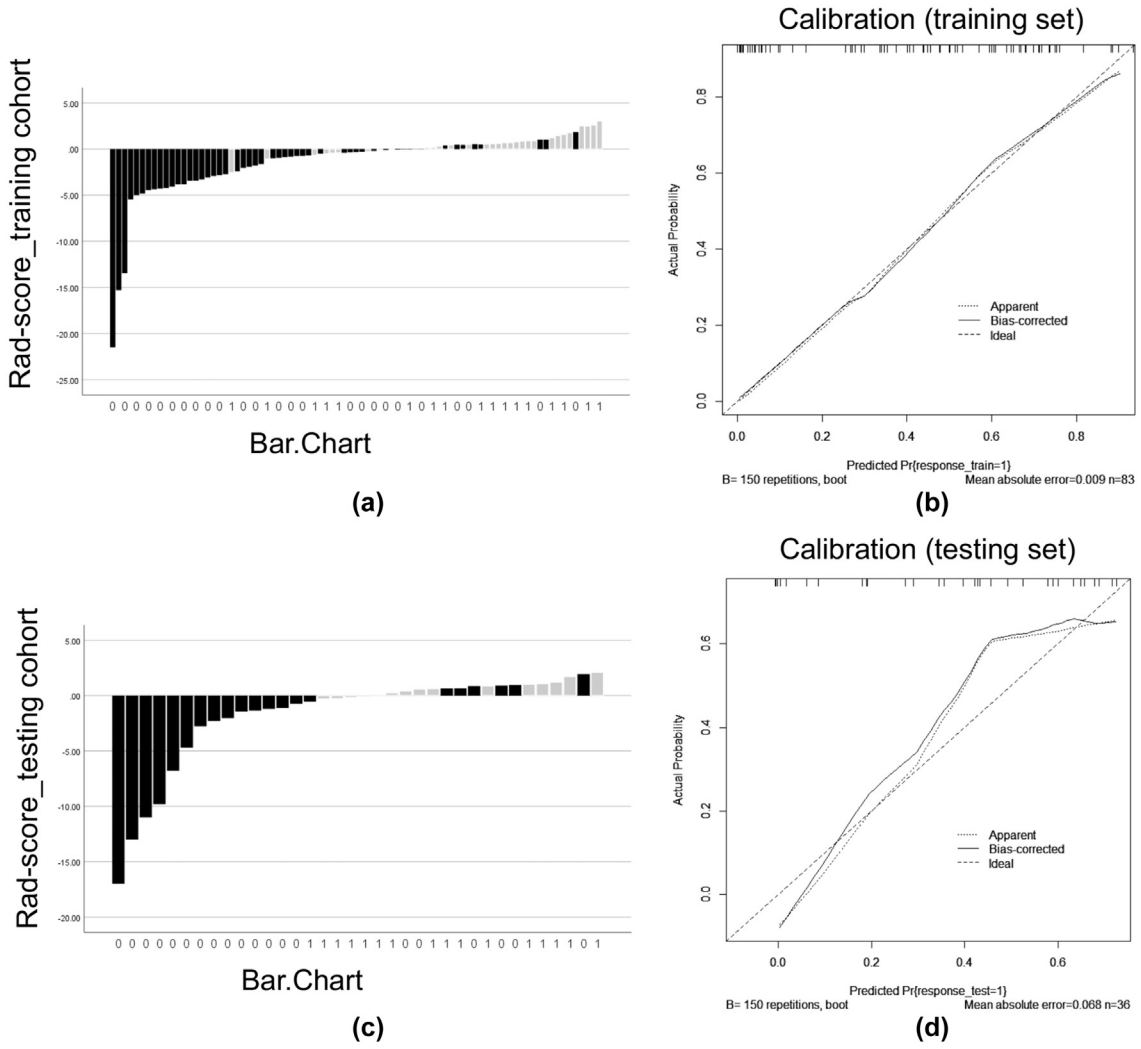

Figure 4 Rad-scores and calibration plots for each patient in the training and testing cohorts. (a,c) Blue bars show the scores for patients who had IAs, while the pink bars show the scores for those who had MIAs. (b,d) The calibration curve of the radiomics score. The diagonal dotted line represents an ideal evaluation, while the solid lines and dashed lines represent the performance of the corrected and apparent bias, respectively. The closer the fit to the diagonal dotted line, the better the evaluation.

discriminating IAs from MIAs in patients with solitary part-solid nodules. The nomogram incorporates four items of the radiomics signature of MaxIntensity, RMS, ZonePercentage, and LongRunEmphasis_angle0_offset7 as well as the lesion shape. Integrating the radiomics signature and CT features into an easy-to-use nomogram facilitates the preoperative individualised diagnosis of part-solid nodules. Moreover, the radiomic biomarkers provided better diagnostic potential than the CT features with a more reliable AUC (0.854 versus 0.755) in discriminating IAs from MIAs.

As the most widely used method for medical imaging, CT provides features such as lesion border, presence of vacuoles, lesion margin, and so forth, for diagnosing disease. Conventional diagnosis relies on those visually identifiable discriminators; however, this process is not an easy or accurate method for identifying the different diseases. In contrast, radiomics is capable of extracting substantially greater numbers of invisible lesion features with much better reproducibility than the conventional method.[33] Recently, a number of studies have utilised radiomics signatures for differentially diagnosing a range of diseases.[32,34–36] To the authors' knowledge, no published study has used a quantitative radiomics model that integrates CT imaging features to distinguish IAs from MIAs that present as solitary part-solid nodules.

In the present study, part-solid nodules with irregular shapes had a greater tendency to be IAs than GGNs with regular shapes, which was in accordance with the results of a previous study.[6] The most likely explanation is that different cancer cells in different areas of the cancer have different differentiation and growth velocities, and the contractions caused by intratumour fibrosis may contribute to the irregular morphology.[37] Conversely, the literature reports that nodular size is a crucial independent predictive factor for identifying IAs and that increases in GGN size will increase the likelihood of malignancy[38]; however, lesion size was ruled out in the multiple logistic regression analysis when it was combined with the radiomic features. The

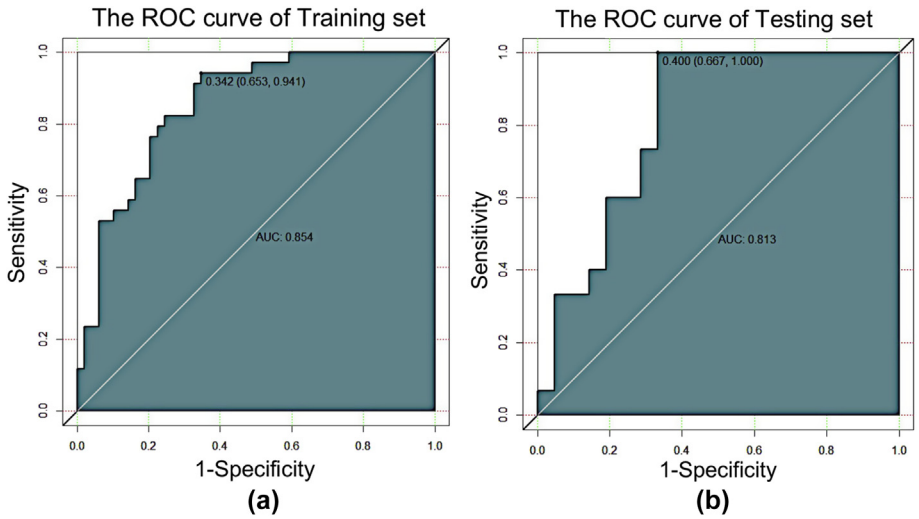

Figure 5 The predictive performance of the radiomic features for distinguishing part-solid nodules as IAs or MIAs from the training and testing cohorts, as presented by ROC curves in (a) the training dataset (AUC = 0.854, 95% CI: 0.774–0.934) and (b) the testing dataset (AUC = 0.813, 95% CI: 0.670–0.955).

reason behind the elimination of lesion size may be that the differences in nodule size between the two histopathologic subtypes were too small. In addition, the inadequate number of patients involved in this study may have resulted in a nonsignificant lesion size. As a consequence, lesion size was not a reliable feature for distinguishing between histopathological subtypes.

Radiomic analysis has offered great potential in identifying the pathological invasiveness of lung adenocarcinomas. Xue *et al.* disclosed that a radiomics model based upon mixed density and fractal dimensions may contribute to differentiating pre-invasive lesions from IAs with good discrimination in both primary and validation cohorts, with AUCs of 0.757 (95% CI: 0.711–0.803) and 0.793 (95% CI: 0.708–0.793), respectively.[39] In the study of Li *et al.*, the authors found that the surface area feature (p=0.040) and the extruded surface area feature (p=0.013) could be predictors of IAs but not of MIAs.[40] Chae *et al.* confirmed that high kurtosis and small mass are significant indicators for distinguishing pre-invasive lesions from IAs in partly solid nodules, but they only focused on 22 features (few of which were texture features such as histogram features, volumetric features, and morphological features).[41] These previously discovered radiomic features are different from those that might be useful in guiding intervention choices for patients with pulmonary nodules.

Based on the preceding studies, the present studies focused on solitary part-solid nodules and acquired 396 features; the four best-performing features were demonstrated to show significant importance including MaxIntensity, RMS (root mean square), Zone Percentage, and LongRunEmphasis_angle0_offset7, all of which allowed us to discriminate between the histopathological subtypes of invasive lesions. The Rad-score was calculated based on the four remaining features after LASSO analysis. A radiomic signature model was constructed with the Rad-score that exhibited high performance with an AUC of 0.854 and 94.1% specificity, but the sensitivity was unsatisfactory. Therefore, a better prediction model was established by combining the lesion shape and Rad-score that successfully demonstrated the greatest performance of the different models.

MaxIntensity and RMS are first-order histogram features that are related to the characteristics of the intensity distribution in the region of interest (ROI). RMS is the square root of the mean of all the squared intensity values. RMS is another measure of the magnitude of the image values. MaxIntensity and RMS have been shown to be significant features for distinguishing pre-invasive lesions from MIAs or IAs.[40] In the present study, MaxIntensity and RMS could be independent indicators for discriminating IAs from MIAs. The zone percentage of GLSZM is the ratio between the total number of zones and the number of voxels in the VOI. It has been observed that the zone percentage of GLSZM is a regional texture feature with the ability to differentiate between patients with various tumours and different prognoses.[42] The RLM-based LoneRunEmphasis is a measure of the distribution of long run lengths, where a high value is indicative of longer run lengths and coarse structural textures. Tixier *et al.* showed that in 41 patients, RLM differentiated between non-responders, partial responders, and complete responders in oesophageal cancer patients.[43] In a study by Cha *et al.*, multiple radiomics features including RLM-based features were demonstrated to be useful in determining the response of bladder carcinomas to systemic chemotherapy.[44] It is noteworthy that no previous study has reported the ZonePercentage of GLSZM and RLM-based LoneRunEmphasis is in lung GGNs. Therefore, we identified novel features that can be applied to distinguish IAs from MIAs in lung GGN patients.

The main limitations were that this was a retrospective study, and only lesions that underwent surgery were chosen, so there may be a selection bias. The study was performed in two institutions, and the different reconstruction algorithms may affect the image quality. Thus, it is

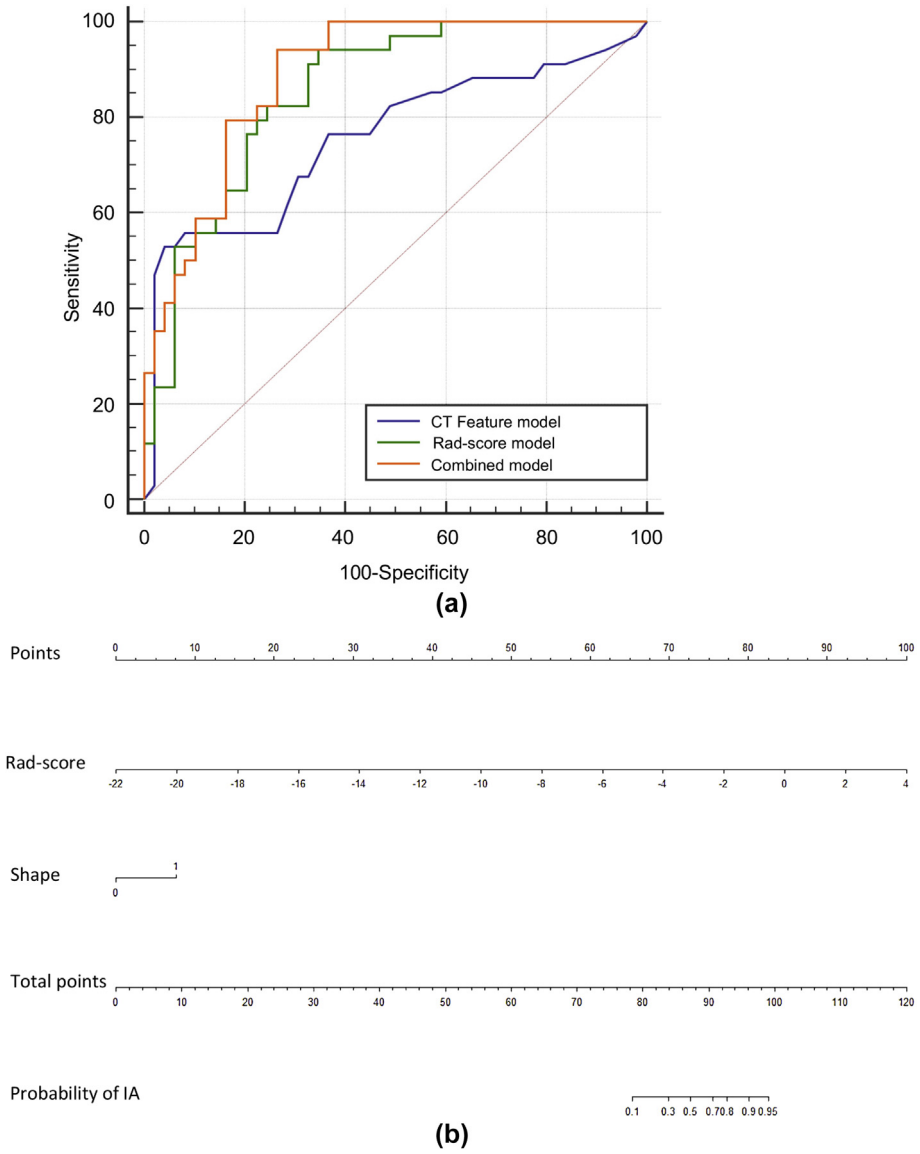

Figure 6 The predictive value of the combined model. (a) The comparison of different signature models to predict the invasiveness of part-solid nodules. (b) A nomogram integrated the radiomic score and lesion shape of the training sets. The probability value of each lesion being an IA is marked on each axis.

necessary to validate the findings in multiple centres. The CT images analysed in the present study were unenhanced, and whether the findings in this study are suitable for enhanced images needs further investigation. Manual segmentation, although regarded as the reference standard, is a labour-intensive and time-consuming process that restricts its extensive application to larger cohorts.

In conclusion, radiomics provides a novel method to extract potentially important data from CT that can define different clusters. Radiomic signatures coupled with CT features can significantly improve the differential diagnosis of IAs and MIAs from part-solid nodules. The quantitative nomogram prediction model based on the Rad-score and lesion shape that was used for the differential diagnosis of IAs and MIAs may serve as an alternative method for precision medicine and provide highly informative data for making clinical management decisions. Moreover, other factors, such as pathological findings of nodal diffusion, may also steer the decision for surgical therapy. Larger study sizes will be needed to confirm the differences in outcomes observed between groups.

Table 3
The diagnostic performances of the radiomic features and morphology features in distinguishing between MIAs and IAs.

	AUC	Sensitivity	Specificity	95% CI	Cut-off
Radiomics signature	0.854	65.3%	94.1%	[0.775, 0.934]	0.342
CT features	0.755	52.9%	95.9%	[0.648, 0.843]	0.768
Combined	0.888	73.5%	94.1%	[0.820, 0.955]	0.500

MIA, minimally invasive adenocarcinoma; IA, Invasive adenocarcinoma; AUC, area under the curve; CI, confidence interval; CT, computed tomography.

Conflict of interest

GE Healthcare kindly provide the A.K. software. Peipei Pang works for GE Healthcare helped us to analysis the data.

Acknowledgements

This study was supported by the National Natural Science Foundation of China (81803778 to L.Z.), The Key Research and Development Project of Zhejiang Province (2018C0302 to J.J.), The Medical and Health Care Key Project of Zhejiang Province (WKJ-ZJ-1629 to J.J.), Zhejiang Medical and Health Science Project (2019RC320 to Q.W.), The Public Welfare Project of Zhejiang Province (LGF18H160035 to H.W.), and the Science and Technology Project of Lishui City (2017ZDXK07 to Z.W.).

References

1. Rittmeyer A, Barlesi F, Waterkamp D, *et al*. Atezolizumab versus docetaxel in patients with previously treated non-small-cell lung cancer (OAK): a phase 3, open-label, multicentre randomised controlled trial. *Lancet* 2017;**389**(10066):255–65.
2. Torre LA, Bray F, Siegel RL, *et al*. Global cancer statistics, 2012. *CA Cancer J Clin* 2015;**65**(2):87–108.
3. Tamura T, Satoh H. Quantitative CT scanning analysis of pure ground-glass opacity nodules predicts further CT change. *Chest* 2016;**149**(6):1586–7.
4. Lee GD, Park CH, Park HS, *et al*. Lung adenocarcinoma invasiveness risk in pure ground-glass opacity lung nodules smaller than 2 cm. *Thorac Cardiovasc Surg* 2018.
5. MacMahon H, Naidich DP, Goo JM, *et al*. Guidelines for management of incidental pulmonary nodules detected on CT images: from the Fleischner Society 2017. *Radiology* 2017;**284**(1):228–43.
6. Wang XW, Chen WF, He WJ, *et al*. CT features differentiating pre- and minimally invasive from invasive adenocarcinoma appearing as mixed ground-glass nodules: mass is a potential imaging biomarker. *Clin Radiol* 2018;**73**(6):549–54.
7. Cohen JG, Reymond E, Lederlin M, *et al*. Differentiating pre- and minimally invasive from invasive adenocarcinoma using CT-features in persistent pulmonary part-solid nodules in Caucasian patients. *Eur J Radiol* 2015;**84**(4):738–44.
8. Mets OM, de Jong PA, Scholten ET, *et al*. Subsolid pulmonary nodule morphology and associated patient characteristics in a routine clinical population. *Eur Radiol* 2017;**27**(2):689–96.
9. Nakamura H, Koizumi H, Kimura H, *et al*. Epidermal growth factor receptor mutations in adenocarcinoma in situ and minimally invasive adenocarcinoma detected using mutation-specific monoclonal antibodies. *Lung Cancer* 2016;**99**:143–7.
10. Lee HY, Lee KS. Ground-glass opacity nodules: histopathology, imaging evaluation, and clinical implications. *J Thorac Imaging* 2011;**26**(2):106–18.
11. Lee SM, Park CM, Goo JM, *et al*. Invasive pulmonary adenocarcinomas versus pre-invasive lesions appearing as ground-glass nodules: differentiation by using CT features. *Radiology* 2013;**268**(1):265–73.
12. Zhang J, Wu J, Tan Q, *et al*. Why do pathological stage IA lung adenocarcinomas vary from prognosis?: a clinicopathologic study of 176 patients with pathological stage IA lung adenocarcinoma based on the IASLC/ATS/ERS classification. *J Thorac Oncol* 2013;**8**(9):1196–202.
13. Fu L, Alam MS, Ren Y, *et al*. Utility of maximum standard uptake value as a predictor for differentiating the invasiveness of T1 stage pulmonary adenocarcinoma. *Clin Lung Cancer* 2018;**19**(3):221–9.
14. Yoshizawa A, Motoi N, Riely GJ, *et al*. Impact of proposed IASLC/ATS/ERS classification of lung adenocarcinoma: prognostic subgroups and implications for further revision of staging based on analysis of 514 stage I cases. *Mod Pathol* 2011;**24**(5):653–64.
15. Anderson KR, Onken A, Heidinger BH, *et al*. Pathologic T descriptor of nonmucinous lung adenocarcinomas now based on invasive tumour size: how should pathologists measure invasion? *Am J Clin Pathol* 2018;**150**(6):499–506.
16. Rios Velazquez E, Parmar C, Liu Y, *et al*. Somatic mutations drive distinct imaging phenotypes in lung cancer. *Cancer Res* 2017;**77**(14):3922–30.
17. Son JY, Lee HY, Kim JH, *et al*. Quantitative CT analysis of pulmonary ground-glass opacity nodules for distinguishing invasive adenocarcinoma from non-invasive or minimally invasive adenocarcinoma: the added value of using iodine mapping. *Eur Radiol* 2016;**26**(1):43–54.
18. Choy G, Khalilzadeh O, Michalski M, *et al*. Current applications and future impact of machine learning in radiology. *Radiology* 2018;**288**(2):318–28.
19. Pinker K. Beyond breast density: radiomic phenotypes enhance assessment of breast cancer risk. *Radiology* 2018:182296.
20. Bae S, Choi YS, Ahn SS, *et al*. Radiomic MRI phenotyping of glioblastoma: improving survival prediction. *Radiology* 2018:180200.
21. Pinker K, Chin J, Melsaether AN, *et al*. Precision medicine and radiogenomics in breast cancer: new approaches toward diagnosis and treatment. *Radiology* 2018;**287**(3):732–47.
22. Gillies RJ, Kinahan PE, Hricak H. Radiomics: images are more than pictures, they are data. *Radiology* 2016;**278**(2):563–77.
23. Kickingereder P, Burth S, Wick A, *et al*. Radiomic profiling of glioblastoma: identifying an imaging predictor of patient survival with improved performance over established clinical and radiologic risk models. *Radiology* 2016;**280**(3):880–9.
24. Coroller TP, Agrawal V, Narayan V, *et al*. Radiomic phenotype features predict pathological response in non-small cell lung cancer. *Radiother Oncol* 2016;**119**(3):480–6.
25. Cohen JG, Reymond E, Jankowski A, *et al*. Lung adenocarcinomas: correlation of computed tomography and pathology findings. *Diagn Interv Imaging* 2016;**97**(10):955–63.
26. Naidich DP, Bankier AA, MacMahon H, *et al*. Recommendations for the management of subsolid pulmonary nodules detected at CT: a statement from the Fleischner Society. *Radiology* 2013;**266**(1):304–17.
27. Lu W, Cham MD, Qi L, *et al*. The impact of chemotherapy on persistent ground-glass nodules in patients with lung adenocarcinoma. *J Thorac Dis* 2017;**9**(11):4743–9.
28. Yue X, Liu S, Liu S, *et al*. HRCT morphological characteristics distinguishing minimally invasive pulmonary adenocarcinoma from invasive pulmonary adenocarcinoma appearing as subsolid nodules with a diameter of </=3 cm. *Clin Radiol* 2018;**73**(4). 411 e417-411 e415.
29. Lee SW, Park H, Lee HY, *et al*. Deciphering clinicoradiologic phenotype for thymidylate synthase expression status in patients with advanced lung adenocarcinoma using a radiomics approach. *Sci Rep* 2018;**8**(1):8968.
30. Feng Q, Chen Y, Liao Z, *et al*. Corpus callosum radiomics-based classification model in Alzheimer's disease: a case–control study. *Front Neurol* 2018;**9**:618.
31. Yang D, Rao G, Martinez J, *et al*. Evaluation of tumour-derived MRI-texture features for discrimination of molecular subtypes and prediction of 12-month survival status in glioblastoma. *Med Phys* 2015;**42**(11):6725–35.
32. Yang X, He J, Wang J, *et al*. CT-based radiomics signature for differentiating solitary granulomatous nodules from solid lung adenocarcinoma. *Lung Cancer* 2018;**125**:109–14.
33. Wilson R, Devaraj A. Radiomics of pulmonary nodules and lung cancer. *Transl Lung Cancer Res* 2017;**6**(1):86–91.
34. Yao Z, Dong Y, Wu G, *et al*. Preoperative diagnosis and prediction of hepatocellular carcinoma: radiomics analysis based on multi-modal ultrasound images. *BMC Cancer* 2018;**18**(1):1089.
35. Guo J, Liu Z, Shen C, *et al*. MR-based radiomics signature in differentiating ocular adnexal lymphoma from idiopathic orbital inflammation. *Eur Radiol* 2018;**28**(9):3872–81.
36. Truhn D, Schrading S, Haarburger C, *et al*. Radiomic versus convolutional neural networks analysis for classification of contrast-enhancing lesions at multiparametric breast MRI. *Radiology* 2018:181352.
37. Gao F, Sun Y, Zhang G, *et al*. CT characterization of different pathological types of subcentimeter pulmonary ground-glass nodular lesions. *Br J Radiol* 2018:20180204.

38. Zhang YP, Heuvelmans MA, Zhang H, *et al*. Changes in quantitative CT image features of ground-glass nodules in differentiating invasive pulmonary adenocarcinoma from benign and in situ lesions: histopathological comparisons. *Clin Radiol* 2018;**73**(5). 504 e509-504 e516.
39. Xue X, Yang Y, Huang Q, *et al*. Use of a radiomics model to predict tumour invasiveness of pulmonary adenocarcinomas appearing as pulmonary ground-glass nodules. *Biomed Res Int* 2018;**2018**:6803971.
40. Li W, Wang X, Zhang Y, *et al*. Radiomic analysis of pulmonary ground-glass opacity nodules for distinction of pre-invasive lesions, invasive pulmonary adenocarcinoma and minimally invasive adenocarcinoma based on quantitative texture analysis of CT. *Chin J Cancer Res* 2018;**30**(4):415–24.
41. Chae HD, Park CM, Park SJ, *et al*. Computerized texture analysis of persistent part-solid ground-glass nodules: differentiation of pre-invasive lesions from invasive pulmonary adenocarcinomas. *Radiology* 2014;**273**(1):285–93.
42. De Bernardi E, Buda A, Guerra L, *et al*. Radiomics of the primary tumour as a tool to improve (18)F-FDG-PET sensitivity in detecting nodal metastases in endometrial cancer. *EJNMMI Res* 2018;**8**(1):86.
43. Tixier F, Le Rest CC, Hatt M, *et al*. Intratumour heterogeneity characterized by textural features on baseline 18F-FDG PET images predicts response to concomitant radiochemotherapy in esophageal cancer. *J Nucl Med* 2011;**52**(3):369–78.
44. Cha KH, Hadjiiski L, Chan HP, *et al*. Bladder cancer treatment response assessment in CT using radiomics with deep-learning. *Sci Rep* 2017;**7**(1):8738.